Open Access Journal
Journal of Power Technologies 94 (1) (2014) 34–41
journal homepage:papers.itc.pw.edu.pl

Non-Newtonian fluid flow in an asymmetric channel with convective surface boundary condition: A note

Noreen Sher Akbar*

DBS&H, CEME, National University of Sciences and Technology
Islamabad, Pakistan

Abstract

The present article deals with the peristaltic flow of a Williamson fluid in an asymmetric channel with convected boundary conditions. The relevant equations have been developed. The solution expression for stream function, temperature profile and pressure gradient are derived using regular perturbation method. Numerical integration has been carried out for pressure rise per wavelength. Plots are prepared and analyzed for various embedded parameters involved into the problem.

Keywords: Peristaltic flow, Convected boundary conditions, Heat transfer, Asymmetric channel, Williamson fluid

1. Introduction

Peristalsis is a series of wave-like muscle contractions that moves food to different processing stations in the digestive tract. The process of peristalsis begins in the esophagus when a bolus of food is swallowed. The strong wave-like motions of the smooth muscle in the esophagus carry the food to the stomach, where it is churned into a liquid mixture called chyme. Peristaltic flows play an important role in sanitary fluid transport, transport of corrosive fluids and toxic liquid transport in the nuclear industry. After the first analysis done by Latham [1], preliminary mathematical models for peristaltic flow in an infinitely long symmetric channel or tube were developed by Shapiro et al. [2]. Several theoretical and experimental investigations have been prepared to exploit the peristaltic action in different flow geometries [3–12].

Convective boundary conditions are basically used to define a linear convective heat exchange condition for one or more geometric entities in Thermal mode. Heat transfer analysis in connection with convective boundary conditions is used in processes such as thermal energy storage, gas turbines, nuclear plants, etc. Aziz [13] presented a similarity solution for Blasius flow of viscous fluid with convective boundary conditions. In another article Makinde and Aziz [14] developed MHD mixed convection flow in a vertical plate in a porous medium in connection with convective boundary conditions. Makinde [15] also discussed the MHD boundary layer flow with heat and mass transfer analysis over a vertical plate with convected boundary conditions. The forced convection heat transfer analysis from the flow of a uniform stream over a flat surface with convective boundary condition is considered by Merkin and Pop [16]. According to them the heat transfer near the leading edge is dominated by the surface heat flux.

*Corresponding author
Email address: noreensher@yahoo.com (Noreen Sher Akbar*)

The aim of the present work is to discuss the peristaltic flow of a Williamson fluid in an asymmetric channel with convective surface boundary conditions. The governing equations were developed and simplified by employing suitable approximations and assumptions. The solution expressions of stream function, longitudinal pressure gradient, temperature profile, pressure rise and frictional forces were calculated. Graphical results are presented in order to illustrate the variations of various parameters.

2. Mathematical formulation

We discussed an incompressible magnetohydrodynamic (MHD) Williamson fluid in an asymmetric channel. The width of channel is taken as $d_1 + d_2$. Flow is induced due to sinusoidal wave propagating with constant speed c on the channel walls. The heat transfer analysis with convected boundary condition is maintained by giving temperatures T_0 and T_1 to the lower and upper walls of a channel correspondingly. The wall surfaces are taken as

$$\begin{aligned} Y = H_1 &= d_1 + a_1 \cos\left[\tfrac{2\pi}{\lambda}(X - ct)\right], \\ Y = H_2 &= -d_2 - b_1 \cos\left[\tfrac{2\pi}{\lambda}(X - ct) + \phi\right], \end{aligned} \tag{1}$$

in the above equations a_1 and b_1 are the waves amplitudes, λ is the wave length, $d_1 + d_2$ is the channel width, c is the wave speed, t is the time, X is the direction of wave propagation and Y is perpendicular to X . The phase difference ϕ varies in the range $0 \le \phi \le \pi$. For $\phi = 0$ the symmetric channel with waves out of phase can be described and when $\phi = \pi$, the waves are in phase. Moreover, a_1, b_1, d_1, d_2 and ϕ fulfill the following relation

$$a_1^2 + b_1^2 + 2a_1 b_1 \cos\phi \le (d_1 + d_2)^2 .$$

The transformations between the laboratory and wave frames are given by

$$x = X - ct,\ y = Y,\ u = U - c,\ v = V,\ p(x) = P(X, t), \tag{2}$$

The stream function Ψ is defined by

$$u = \frac{\partial \Psi}{\partial y}, \quad v = -\delta \frac{\partial \Psi}{\partial x} \tag{3}$$

satisfies the continuity equation identically. Dimensionless variables are defined by

$$\begin{gathered} \bar{x} = \tfrac{2\pi x}{\lambda},\ \bar{y} = \tfrac{y}{d_1},\ \bar{u} = \tfrac{u}{c},\ \bar{v} = \tfrac{v}{c\delta},\ \delta = \tfrac{d_1}{\lambda},\ d = \tfrac{d_2}{d_1}, \\ \bar{P} = \tfrac{d_1^2 P}{\mu c \lambda},\ h_1 = \tfrac{H_1}{d_1},\ \bar{t} = \tfrac{ct}{\lambda},\ h_2 = \tfrac{H_2}{d_2},\ a_2 = \tfrac{a_1}{d_1},\ b = \tfrac{b_1}{d_1}, \\ R = \tfrac{cd_1}{\nu},\ \bar{\Psi} = \tfrac{\Psi}{cd_1},\ \theta = \tfrac{T - T_0}{T_1 - T_0},\ E_c = \tfrac{c^2}{c_p(T_1 - T_0)}, \\ P_r = \tfrac{\rho \nu c_p}{K'},\ \bar{S} = \tfrac{S d_1}{\mu c},\ We = \tfrac{\Gamma c}{d_1},\ M = \sqrt{\tfrac{\sigma}{\mu}} B_0 d_1. \end{gathered} \tag{4}$$

The flow equations for Williamson fluid in dimensionless form under long wave length and low Reynold's number approximation takes the form [6]

$$\frac{\partial^2}{\partial y^2}\left[\frac{\partial^2 \Psi}{\partial y^2} + We\left(\frac{\partial^2 \Psi}{\partial y^2}\right)^2 - M^2 \Psi\right] = 0, \tag{5}$$

$$\frac{dP}{dx} = \frac{\partial}{\partial y}\left[\frac{\partial^2 \Psi}{\partial y^2} - M^2 \Psi + We\left(\frac{\partial^2 \Psi}{\partial y^2}\right)^2\right], \tag{6}$$

$$\frac{\partial^2 \theta}{\partial y^2} = -B_r\left[\left(\frac{\partial^2 \Psi}{\partial y^2}\right)^2 + We\left(\frac{\partial^2 \Psi}{\partial y^2}\right)^3\right], \tag{7}$$

where M is the Hartman number, We the Weissenberg number, B_r the Brinkman number and Pr the Prandtl number.

The corresponding boundary conditions can be put into the following forms:

$$\begin{gathered} \Psi = \tfrac{F}{2},\ \tfrac{\partial \Psi}{\partial y} = -1,\ \theta'(h_1) - B_i \theta(h_1) = -B_i, \\ at\ y = h_1 = 1 + a\cos x, \end{gathered} \tag{8}$$

$$\begin{gathered} \Psi = -\tfrac{F}{2},\ \tfrac{\partial \Psi}{\partial y} = -1,\ \theta = 0, \\ at\ y = h_2 = -d - b\cos(x + \phi), \end{gathered} \tag{9}$$

where $B_i = \frac{h_f d_1}{K}$ is the Biot number and h_f is the convective heat transfer coefficient.

The expression relating the time mean flow rate Θ (in the fixed frame) and Q (in the wave frame) is

$$Q = \Theta + 1 + d. \tag{10}$$

3. Series Solutions

For small Weissenberg number We series solutions can be written as follows

$$\Psi = \Psi_0 + W_e\Psi_1 + O\left(W_e^2\right), \tag{11}$$

$$\frac{dP}{dx} = \frac{dP_0}{dx} + W_e\frac{dP_1}{dx} + O\left(W_e^2\right), \tag{12}$$

$$Q = Q_0 + W_eQ_1 + O\left(W_e^2\right), \tag{13}$$

$$\theta = \theta_0 + W_e\theta_1 + O\left(W_e^2\right). \tag{14}$$

Putting the above equations into Eqs. (5)–(9) and then solving the resulting systems we have

$$\begin{aligned}\Psi(x,\,y) = {} & \frac{(L_1+L_2)\cosh My}{M^2} + \frac{(L_1-L_2)\sinh My}{M^2} + L_3y + L_4 \\ & + W_e\left(\frac{(L_5+L_6)\cosh My}{M^2} - \frac{\left(L_1^2+L_2^2\right)\cosh 2My}{3M^2}\right. \\ & \left. + \frac{(L_5-L_6)\sinh My}{M^2} - \frac{\left(L_1^2+L_2^2\right)\sinh 2My}{3M^2}\right),\end{aligned} \tag{15}$$

$$\frac{dP}{dx} = -L_3M^2 + W_e^2\left(-L_8M^2\right), \tag{16}$$

$$\begin{aligned}\theta(x,\,y) = {} & -\frac{B_r(2My(L_1^2-L_2^2+2L_1L_2My+\left(L_1^2+L_2^2\right)\cosh 2My+\left(L_1^2-L_2^2\right)\sinh 2My}{4M^2} \\ & L_{21}y + L_{22} + W_e^2\left(1/108M^4(B_r(48L_1^2L_2^2M^2y^2 + 108L_5L_6M^2y^2\right. \\ & -54L_8^2M^4y^2 - 3L_1^4\cosh 4My - 3L_2^4\cosh 4My - 36(4L_2^2L_5 \\ & -6L_8L_6M + 9L_1L_2^2M^2)\cosh My - \sinh My) - 36(4L_1^2L_6 \\ & +6L_8L_5M + 9L_1^2L_2M^2)(\cosh My + \sinh My) - 9(3L_6^2 \\ & +4L_2^2L_8M)(\cosh 2My - \sinh 2My) - 9\left(3L_5^2 - 4L_1^2L_8M\right) \\ & (\cosh 2My + \sinh 2My) - 4L_2^2\left(-4L_6 + 3L_2M^2\right) \\ & (\cosh 3My - \sinh 3My) - 4L_1^2\left(-4L_5 + 3L_1M^2\right) \\ & \left.(\cosh 3My + \sinh 3My) - 3L_1^4\sinh 4My + 3L_2^4\sinh 4My)\right) \\ & +L_{26}y + L_{27}),\end{aligned} \tag{17}$$

where values of $L_1 - L_{25}$ were calculated using Mathematica.

Heat transfer coefficient Z at the upper wall is defined as

$$Z = (h_1)_x\,\theta(x,\,y)_y\,. \tag{18}$$

and the expression for dimensionless pressure rise ΔP is

$$\Delta P = \int_0^1 \left(\frac{dP}{dx}\right) dx. \tag{19}$$

4. Results and discussion

This section describes the pressure rise, pressure gradient, velocity, temperature and streamlines. The pressure rise per wavelength was examined through numerical integration. The pressure rise against volume flow rate is shown in Figs. 1(a) to 1(c). Basically the pressure rise and volume flow rate have opposite results. Figs. 1(a) to 1(c) showed that in pumping region ($\Delta P > 0$), the pressure rise increases when Weissenberg number We, Hartman number M and amplitude ratio a increase and augmented pumping occurs for ($\Delta P < 0$). Figs. 1(a) to 1(c), show that the pressure rise decreases by increasing the Weissenberg number We, Hartman number M and amplitude ratio a in the augmented pumping region. Free pumping region corresponds ($\Delta P = 0$) . Variations of Hartman number M , Weissenberg number We and flow rate Q on the velocity profile are shown in the Figs. 2(a) to 2(c). Fig. 2(a) shows that the velocity near the channel walls is not similar in view of the Hartman number M . The velocity decreases by increasing M . The velocity for the Weissenberg number was plotted in the Fig. 2(b). It is found that the velocity field increases in the region $y \in [-1.3,\, 0]$, whereas it decreases in region $y \in [0.1, -1.1]$ when the Weissenberg number We increases. Fig. 2(c) shows that an increase in flow rate Q increases the velocity field. The variation of temperature profile for different values of Biot number B_i, Weissenberg number We, Hartman number M and Brinkman number B_r are plotted in Figs. 3(a) to 3(d). Here the temperature profile increases when Biot number B_i, Weissenberg number We and Brinkman number B_r increase. Temperature profile decreases with the increase in Hartman number M.

Figs. 4(a) to 4(c) display the pressure gradient for different values of We, M and a The magnitude of pressure gradient increases with the increase in M, We and a It is also observed that the maximum pressure gradient occurs when $x = 0.48$.

The trapping for different values of M, We, a and Q are shown in Figs. 5(a) to 5(h). It is seen from Figs. 5(a, b) that the size of the trapping bolus decreases by increasing M (in the upper and lower parts of the channel). Figs. 5(c, d) denote that the size and

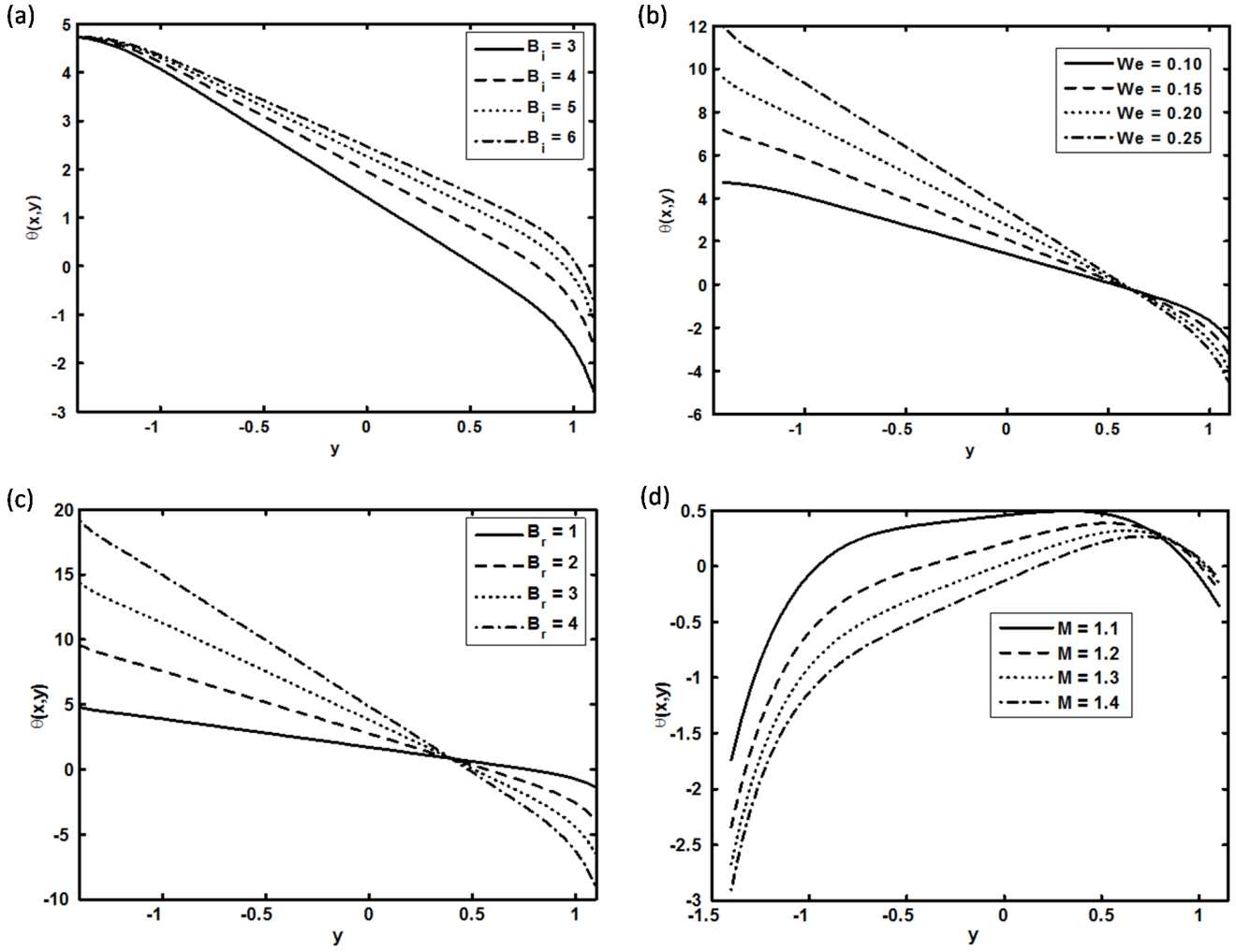

Figure 3: Variation of temperature profile for (a) $a = 0.1$, $b = 0.5$, $d = 1$, $\phi = 0.7$, $x = 1$, $Q = 2$, $B_r = 2$, $M = 2$ and $W_e = 0.1$. (b) $a = 0.1$, $b = 0.5$, $d = 1$, $\phi = 0.7$, $x = 1$, $Q = 2$, $B_r = 2$, $M = 2$ and $B_i = 0.1$. (c) $a = 0.1$, $b = 0.5$, $d = 1$, $\phi = 0.7$, $x = 1$, $Q = 2$, $B_i = 0.2$, $M = 2$ and $W_e = 0.1$. (d) $a = 0.1$, $b = 0.5$, $d = 1$, $\phi = 0.7$, $x = 1$, $Q = 2$, $B_r = 2$, $B_i = 0.2$ and $W_e = 0.1$.

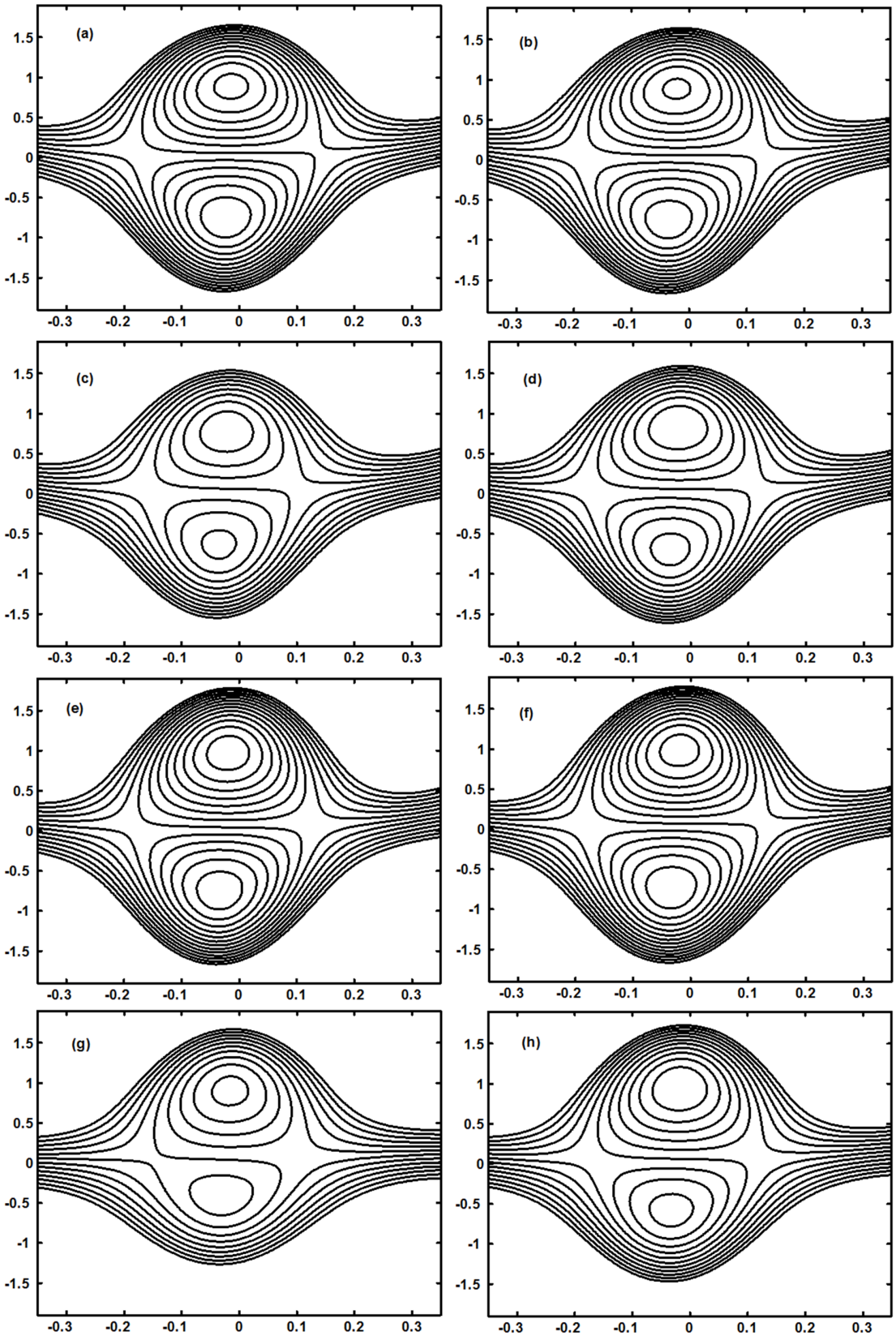

Figure 5: Stream lines for panels ((a) and (b)) for $M = 0.2, 0.4$, ((c) and (d)) for $We = 0.1, 0.2$, ((e) and (f)) for $a = 0.2, 0.3$, ((g) and (h)) for $Q = -2, -3$, while the others parameters are $d = 1$, $\phi = 0.2$, $b = 0.2$.

number of the trapping bolus increases with an increase in We (in the upper and lower parts of the channel). Figs. 5(e, f) show that due to an increase in amplitude ratio a the size and number of bolus increases. It is seen from Figs. 5(e, f) that the size and number of bolus in the upper and lower parts of channel increases when Q increases.

5. Concluding remarks

The present work discusses the Williamson fluid in an asymmetric channel with convected boundary conditions. The main points of the present analysis are as follows.

1. Pressure rise increases when Weissenberg number We, Hartman number M and amplitude ratio a increases.
2. The velocity decreases by increasing M.
3. Velocity profile increases in view of an increase in We and Q.
4. The temperature profile increases when Biot number B_i, Weissenberg number We and Brinkman number B_r increases.
5. The magnitude of pressure gradient increases with the increase in M, We and a
6. The size of the trapping bolus decreases by increasing M (in the upper and lower parts of the channel).
7. The size and number of the trapping bolus increases with an increase in We (in the upper and lower parts of the channel).
8. Due to an increase in amplitude ratio ratio a the size and number of bolus increases.
9. The size and number of bolus in the upper and lower parts of channel increases when Q increases.

References

[1] T. W. Latham, Fluid motion in a peristaltic pump, Master's thesis, Massachusetts Institute of Technology, Cambridge (1966).

[2] A. H. Shapiro, M. Y. Jaffrin, S. L. Weinberg, Peristaltic pumping with long wave lengths at low reynolds numbers, Journal of Fluid Mechanics 37 (1969) 799–825.

[3] K. Mekheimer, Y. A. elmaboud, The influence of heat transfer and magnetic field on peristaltic transport of a newtonian fluid in a vertical annulus: Application of an endoscope, Physics Letters A 372 (10) (2008) 1657–1665. doi:http://dx.doi.org/10.1016/j.physleta.2007.10.028.

[4] K. S. Mekheimer, Effect of the induced magnetic field on peristaltic flow of a couple stress fluid, Physics Letters A 372 (2008) 4271–4278.

[5] M. H. Haroun, Non-linear peristaltic flow of a fourth grade fluid in an inclined asymmetric channel, Computational Materials Science 39 (2007) 324–333.

[6] N. S. Akbar, S. Nadeem, T. Hayat, S. Obaidat, Peristaltic flow of a williamson fluid in an inclined asymmetric channel with partial slip and heat transfer, International Journal of Heat and Mass Transfer 55 (2012) 1855–1862.

[7] S. Srinivas, R. Gayathri, Peristaltic transport of a newtonian fluid in a vertical asymmetric channel with heat transfer and porous medium, Applied Mathematics and Computation 215 (2009) 185–196.

[8] A. Yldrm, S. A. Sezer, Effects of partial slip on the peristaltic flow of a mhd newtonian fluid in an asymmetric channel, Mathematical and Computer Modelling 52 (2010) 618–625.

[9] S. Srinivas, R. Gayathri, M. Kothandapani, The influence of slip conditions, wall properties and heat transfer on mhd peristaltic transport, Computer Physics Communications 180 (2009) 2115–2122.

[10] S. Srinivas, M. Kothandapani, The influence of heat and mass transfer on mhd peristaltic flow through a porous space with compliant walls, Applied Mathematics and Computation 213 (2009) 197–208.

[11] D. Tripathi, Mathematical model for the peristaltic flow of chyme movement in small intestine, Mathematical Biosciences 233 (2011) 90–97.

[12] D. Tripathi, Peristaltic transport of fractional maxwell fluids in uniform tubes: Applications in endoscopy, Computers & Mathematics with Applications 62 (2011) 1116–1126.

[13] A. Aziz, A similarity solution for laminar thermal boundary layer over a flat plate with a convective surface boundary condition, Communications in Nonlinear Science and Numerical Simulation 14 (2009) 1064–1068.

[14] O. D. Makinde, A. Aziz, Mhd mixed convection from a vertical plate embedded in a porous medium with a convective boundary condition, International Journal of Thermal Sciences 49 (2010) 1813–1820.

[15] O. D. Makinde, Similarity solution of hydromagnetic heat and mass transfer over a vertical plate with a convective surface boundary condition, International Journal of Physical Sciences 5 (6) (2010) 700–710.

[16] J. H. Merkin, I. Pop, The forced convection flow of a uniform stream over a flat surface with a convective surface boundary condition, Communications in Nonlinear Science and Numerical Simulation 16 (2011) 3602–3609.

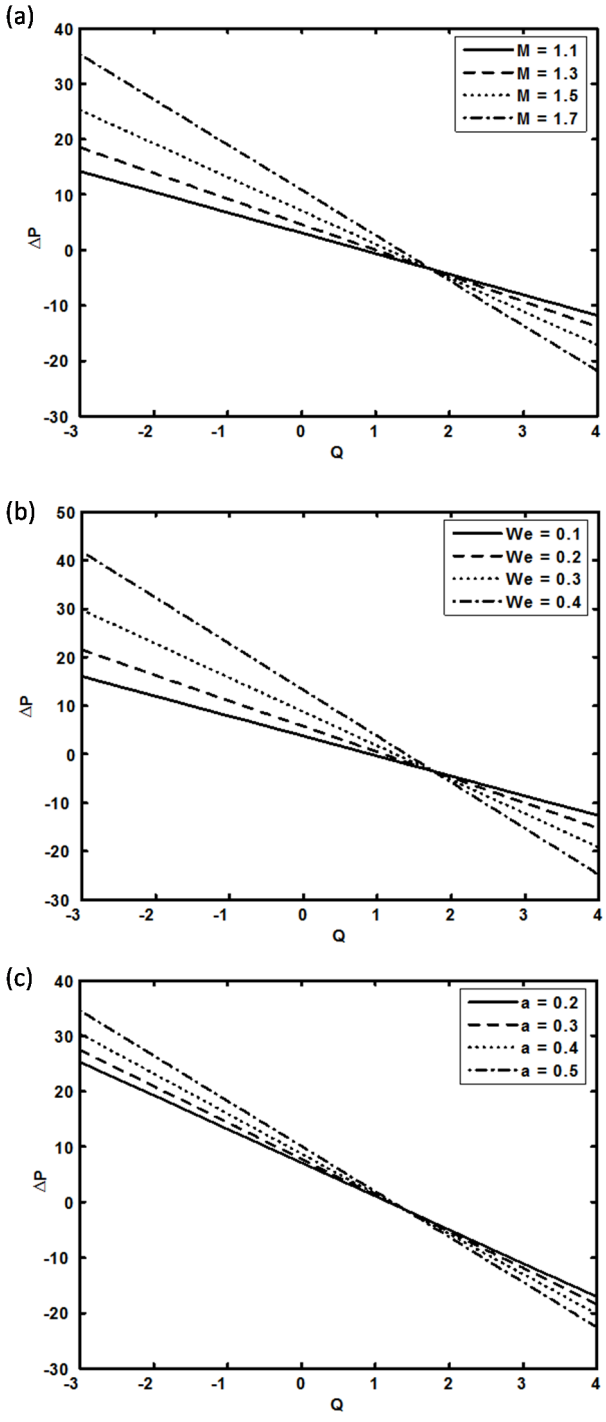

Figure 1: Variation of pressure rise versus flow rate for (a) $a = 0.2$, $b = 0.7$, $d = 1$, $\phi = 0.7$ and $W_e = 0.2$. (b) $a = 0.3$, $b = 0.7$, $d = 1$, $\phi = 0.7$ and $M = 2$. (c) $W_e = 0.3$, $b = 0.7$, $d = 1$, $\phi = 0.7$ and $M = 2$.

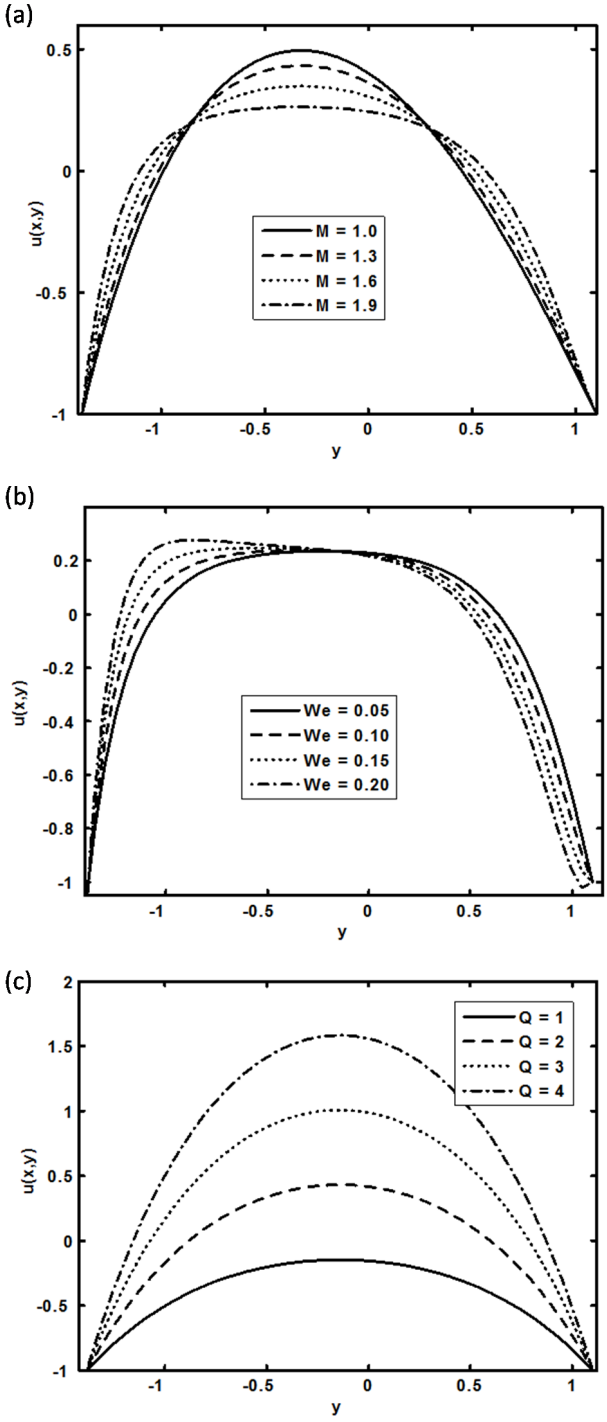

Figure 2: Variation of velocity profile for (a) $a = 0.1$, $b = 0.5$, $d = 1$, $\phi = 0.7$, $x = 1$, $Q = 2$ and $W_e = 0.2$. (b) $a = 0.1$, $b = 0.5$, $d = 1$, $\phi = 0.7$, $x = 1$, $Q = 2$ and $M = 0.2$. (c) $a = 0.1$, $b = 0.5$, $d = 1$, $\phi = 0.7$, $x = 1$, $W_e = 0.2$ and $M = 0.2$.

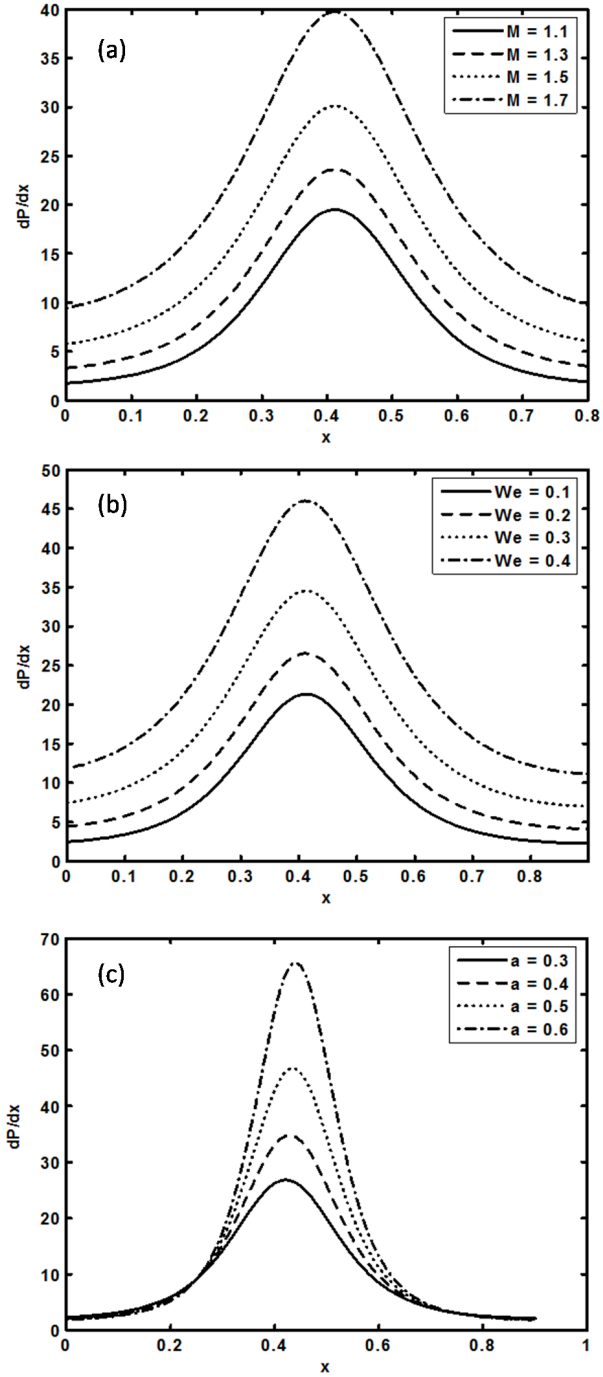

Figure 4: Variation of pressure gradient for (a) $a = 0.2$, $b = 0.7$, $d = 1$, $\phi = 0.7$, $W_e = 0.4$, $Q = -1$. (b) $a = 0.2$, $b = 0.7$, $d = 1$, $\phi = 0.7$, $M = 2$, $Q = -1$. (c) $W_e = 0.2$, $b = 0.7$, $d = 1$, $\phi = 0.7$, $M = 2$, $Q = -1$.